[6]Crossley, W. A., Cook, A. M., Fanjoy, D. W., "Using the Two-Branch Tournament Genetic Algorithm for Multiobjective Design," *AIAA Journal*, Vol. 37, No. 2, 1999, pp. 261–267.

[7]Vicini, A., and Quagliarella, D., "Inverse and Direct Airfoil Design Using a Multiobjective Genetic Algorithm," *AIAA Journal*, Vol. 35, No. 9, 1997, pp. 1499–1505.

[8]Jones, B. R., Crossley, W. A., and Lyrintzis, A., "Aerodynamic and Aeroacustic Optimization of Rotorcraft Airfoils via a Parallel Genetic Algorithm," *Journal of Aircraft*, Vol. 37, No. 6, 2000, pp. 1088–1096.

[9]Obayashi, S., Yamaguchi, Y., and Nakamura, T., "Multiobjective Genetic Algorithm for Multidisciplinary Design of Transonic Wing Planform," *Journal of Aircraft*, Vol. 34, No. 5, 1997, pp. 690–693.

[10]Blasi, L., Iuspa, L., and Del Core, G., "Conceptual Aircraft Design Based on a Multiconstraint Genetic Optimizer," *Journal of Aircraft*, Vol. 37, No. 2, 2000, pp. 350–354.

[11]Obayashi, S., "Pareto Genetic Algorithm for Aerodynamic Design Using the Navier–Stokes Equation," *Genetic Algorithms in Engineering and Computer Science*, Wiley, New York, 1997, pp. 245–266.

Flow Past an Airfoil with a Leading-Edge Rotation Cylinder

X. Du* and T. Lee†
McGill University, Montreal, Quebec H3A 2K6, Canada
F. Mokhtarian** and F. Kafyeke††
Bombardier Aerospace, Dorval, Quebec H4S 1Y9, Canada

Introduction

THE delay of boundary-layer separation and the enhancement of the lift-to-drag ratio of an airfoil are always of great importance, not only to the design of advanced aircraft, but also to the control of the boundary-layer flow. Experimental control schemes, such as suction, blowing, vortex generators, turbulence augmentation, and the use of a moving wall[1–13] have been employed with varied degrees of success. By use of an airfoil with upper surface formed by a belt moving over two rollers, Favre[1] successfully delayed the boundary-layer separation up to an angle of attack α of 58 deg and obtained a maximum lift coefficient $C_{l\,\max}$ of 3.5. Steele and Harding[3] studied the use of rotating cylinders to improve ship maneuverability, using flow visualization and force measurements. Tennant et al.[4] conducted tests with a wedge-shaped flap having a rotating cylinder as the leading edge. Tennant et al.[5] also tested the circulation control for a symmetrical airfoil with a rotating cylinder at the trailing edge and reported that, at a zero angle of attack, a coefficient of lift of 1.2 was obtained for a normalized cylinder rotation, Ω (equal to u_s/u_∞, where u_s is the cylinder surface speed and u_∞ is the freestream velocity) of 1.2. It is now clear that moving-surface boundary-layer control involves the reduction of the initial boundary-layer growth by minimizing the relative velocity between the cylinder surface and the freestream and that, through the retardation of the initial boundary-layer growth and the subsequent delay of the separation of the boundary layer, increases in circulation and lift can then be achieved. Recently, Modi et al.[10] investigated the potential of application of a rotating cylinder at the leading edge of the airfoil of high-lift standard takeoff and landing-type aircraft. The effectiveness of moving-surface boundary-layer control on a symmetrical Joukowsky airfoil has been studied at length[6–12] through surface pressure measurement and flow visualization methods, as well as a six-axis force balance. An excellent review on the moving-surface boundary-layer control is given by Modi.[12]

In summary, the potential of a leading-edge rotating cylinder (LERC) as a boundary-layer control device has been investigated by researchers elsewhere; however, most of the work has focused primarily on exploratory studies or force measurements. No quantitative information of the effects of the cylinder rotation on the fluid dynamics process, especially the behavior of the boundary layer and the wake structure, was documented. The main objective of this study was to measure and characterize the effects of a LERC on the growth, development, and separation of the boundary layers and wake structures developed on and behind a symmetric airfoil by using hot-wire anemometry and smoke-flow visualization methods. Surface pressure measurements were also made to quantify the variation of lift-to-drag ratio under the influence of cylinder rotation. The present measurements provide typical data for computer model validation.

Experimental Apparatus and Methods

The experiments were conducted in a $0.9 \times 1.2 \times 2.7$ m suction-type wind tunnel. The freestream turbulence intensity was 0.04% at $u_\infty = 30$ m/s. A NACA 0015 airfoil with a chord length c of 25.4 cm and a span of 38 cm, fabricated from a solid aluminum, was used as the test model. The airfoil was fitted with endplates to ensure a two-dimensional flow around the airfoil. The leading-edge region of the airfoil was specially designed to accommodate the LERC of a diameter $d = 0.1\,c$ and a length of 38 cm, as well as the base airfoil, that is, airfoil with no leading-edge modification, Fig. 1. The selection of the rather large cylinder diameter in comparison to the leading-edge radius ($r = 0.0248c$) of the base airfoil was based on the consideration of achieving a value of Ω as high as possible. The gap between the rotating cylinder and the main airfoil was set at 1.2 mm. The selection of the present gap size was based on the guidelines suggested by Tennant et al.[5] They reported that a gap size less than 3 mm wide is required to minimize any possible negative effects induced by the

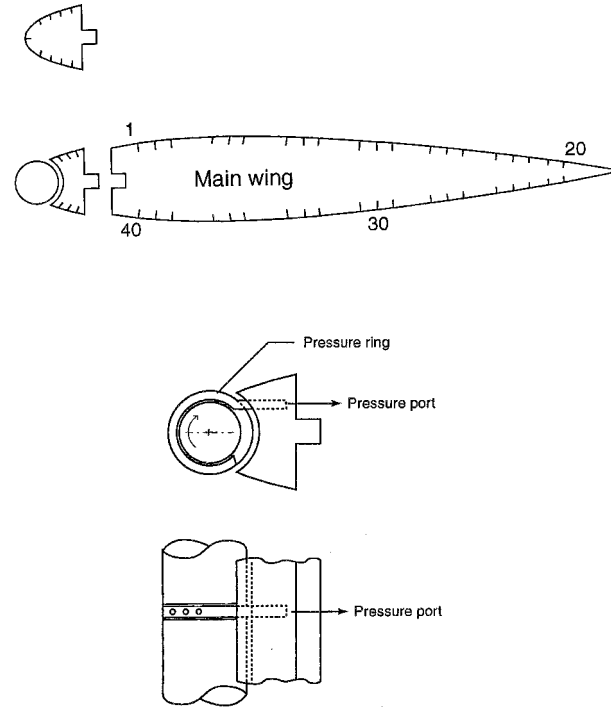

Fig. 1 Schematics of NACA 0015 airfoil model and the details of the pressure taps.

Received 24 January 2002; revision received 15 June 2002; accepted for publication 7 July 2002.

*Graduate Research Assistant, Aerodynamics Laboratory, Department of Mechanical Engineering.

†Associate Professor, Aerodynamics Laboratory, Department of Mechanical Engineering. Member AIAA.

**Section Chief, Advanced Aerodynamics. Member AIAA.

††Manager, Advanced Aerodynamics. Member AIAA.

cylinder rotation. The cylinder was rotated by a $\frac{1}{5}$-hp variable-speed ac motor with an accuracy of ± 20 rpm. The main body of the airfoil model was fitted with 40 0.35-mm pressure orifices, staggered 2 mm apart in the spanwise direction to avoid the wake effect on an upstream orifice on orifices further downstream. The pressure signals were measured with a pressure transducer (Datametric Model 504) in connection with a 48-port Scanivalve system, and were low-pass filtered and sampled at 2 kHz. The pressure on the surface of the rotating cylinder (typically rotated in the range of 2000 to 8000 rpm), which represents the crucial high suction pressure, was obtained by measuring the pressure in the vicinity of the cylinder rather than on the surface itself.[6,10] This was achieved by keeping the pressure taps stationary while the cylinder rotated. When the pressure taps were located in a narrow 2-mm square tube (a width much smaller than the length of the cylinder), it was possible to ensure the continuity of the flow over the entire surface and obtain an estimate of the surrounding pressure. The LERC was provided with a groove to house the "pressure ring" while maintaining the uniformity of the cylinder surface.

The boundary-layer velocity profiles were measured with a 5-μm hot-wire probe (DISA P11) and an AA Lab AN-2000 constant-temperature anemometer. The overheat ratio was set at 1.3 to minimize the effects of the proximity of the airfoil surface.[14] The hot-wire probe was positioned at desired y positions by a computer-controlled traversing mechanism mounted on a moveable guide plate following the contour of the test airfoil. The initial hot-wire probe location y_0, above the airfoil surface, was measured with a cathethometer. The origins of the xy coordinate were located at the leading edge of the airfoil. All hot-wire calibration, freestream turbulence levels, and mean and rms velocity measurements were performed on a 586 personal computer with a 16-bit analog-to-digital converter board. The low speed (0.3–1.5 m/s) hot-wire calibration was performed in the subsonic wind tunnel by the use of the vortex-shedding method suggested by Lee and Budwig.[15] The calibration before and after each test run was reproduced to within 2% of each other. A nichrome wire of 50-μm diam, coated with glycerol, was used to visualize the overall flow patterns around the airfoil. The smoke-flow patterns were illuminated by two 150-W flood lamps and were recorded with a 60-Hz video camera at a shutter speed of $\frac{1}{500}$ s. The effects of cylinder rotation on the flow separation and reattachment were also examined in a smoke tunnel.

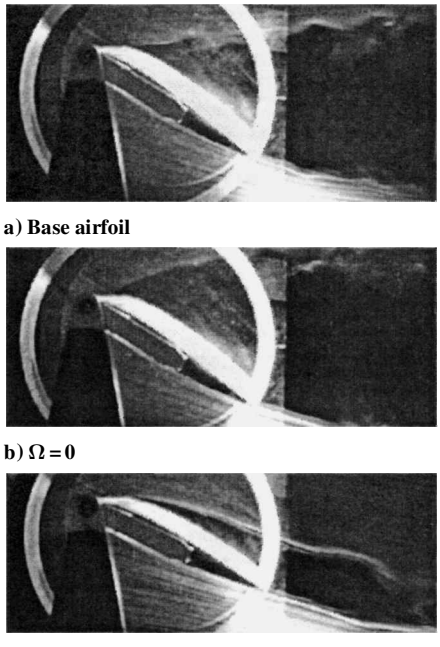

a) Base airfoil

b) $\Omega = 0$

c) $\Omega = 4$

Fig. 2 Typical flow visualization results for $\alpha = 28$ deg.

Results and Discussion

Figure 2 shows the typical smoke-flow patterns for $\alpha = 28$ deg at $Re_c = 1.65 \times 10^4$. The flow is from left to right. The results show that with $\Omega = 0$ (Fig. 2b), the presence of the LERC ($d = 0.1c$) disturbed the boundary-layer flow in the leading-edge region of the airfoil, promoted the flow separation, and resulted in a widened wake and a premature stall as compared to those of a base airfoil (Fig. 2a). With $\Omega = 4$, the smoke streak lines on the top surface moved closer to the airfoil surface and resulted in a delayed flow separation and a narrowed wake (Fig. 2c). The flow visualization results also reveal that, for $\alpha > 28$ deg, the flow remained separated in the leading-edge region. That is, there existed a critical rotation speed ($\Omega > 5$ in the present experiment) beyond which momentum injection through a leading-edge cylinder rotation appeared to have little effect. For $\alpha \leq 10$ deg and $\Omega < 4$, the overall flow patterns were found to be similar to that of a base airfoil. Also, depending on the values of Ω and α, the unsteady flow over the airfoil could be separating and reattaching over a large portion of the top surface of the airfoil.

Figures 3a, 3b, and 3c show the representative effects of cylinder rotation ($\Omega = 0$–1.5) on the airfoil wake velocity profiles (at $x/c = 1.5$) and surface pressure distributions for $\alpha = 16$ deg and $Re_c = 1.65 \times 10^5$, respectively. The selection of the values of Ω was decided based on the experimental limitations imposed by the test flow speed, as well as on the smoke-flow visualization results, which suggested that at $\Omega = 1$, the behavior of the stall and boundary layer could be significantly affected. Figures 3a and 3b show that with increasing cylinder rotation, the significant reduction in

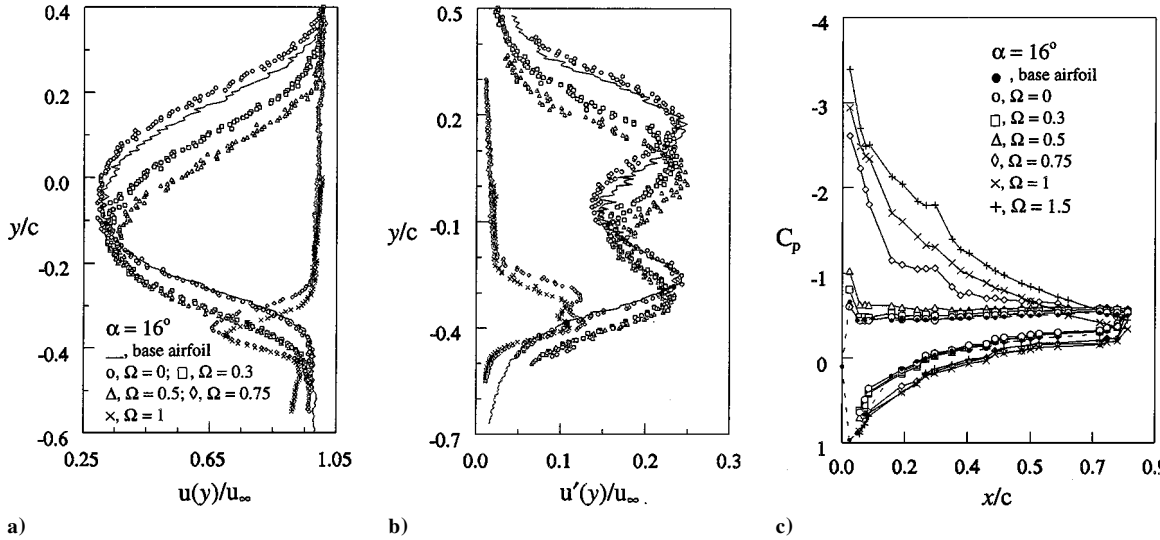

Fig. 3 Wake a) mean and b) fluctuating velocity profiles and c) C_p distributions for $\alpha = 16$ deg.

Table 1 Effect of Ω on normalized wake δ'_w and (θ'_w) at different α

	α, deg								
Location	2	4	6	8	10	12	14	16	18
Base airfoil									
	0.873	0.833	1.015	1.133	1.247	1.600	1.800	5.367	5.633
	(0.063)	(0.050)	(0.052)	(0.060)	(0.080)	(0.096)	(0.241)	(0.924)	(1.047)
LERC airfoil									
Ω = 0	0.827	1.017	1.600	1.853	2.033	4.320	4.400	5.500	5.700
	(0.065)	(0.072)	(0.097)	(0.135)	(0.159)	(0.499)	(0.795)	(0.940)	(1.029)
Ω = 0.3	0.653	0.967	1.550	1.700	1.967	2.300	4.301	5.333	5.667
	(0.064)	(0.067)	(0.087)	(0.109)	(1.124)	(0.238)	(0.732)	(0.911)	(1.005)
Ω = 0.5	0.650	0.997	1.467	1.547	1.467	2.233	2.533	5.200	5.567
	(0.067)	(0.069)	(0.071)	(0.095)	(0.098)	(0.154)	(0.218)	(0.845)	(0.958)
Ω = 0.75	0.753	1.100	1.500	1.747	1.487	1.833	2.000	2.267	5.433
	(0.070)	(0.089)	(0.090)	(0.123)	(0.123)	(0.150)	(0.167)	(0.268)	(1.087)
Ω = 1	0.613	0.897	1.173	1.653	1.367	1.700	1.900	2.067	2.133
	(0.064)	(0.060)	(0.068)	(0.078)	(0.087)	(0.097)	(0.112)	(0.195)	(0.201)

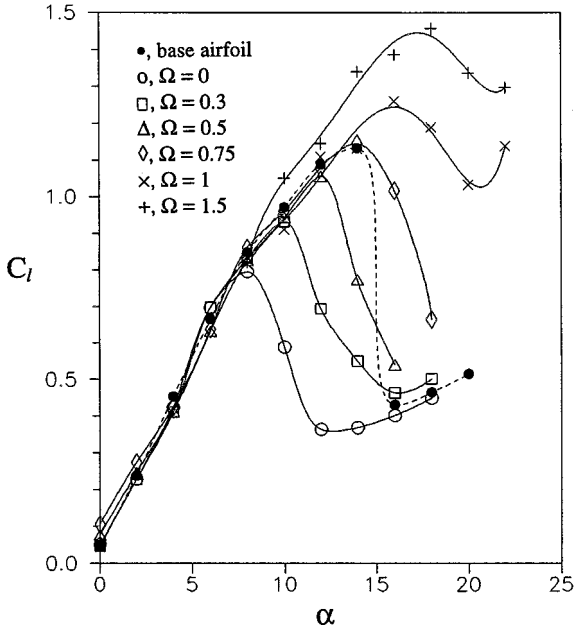

Fig. 4 Effect of Ω on C_l.

the wake width and the associated turbulence strength are apparent in comparison to those of a base airfoil. At $\alpha = 16$ deg and with $\Omega \geq 0.75$, the completely separated flow reattached onto the trailing edge of the airfoil. A reduction of wake width of 190% at $\Omega = 1$ compared to that of a base airfoil was observed. The variations of the normalized wake width δ'_w (equal to δ_w/t, where t is the maximum thickness of the airfoil) and momentum thickness θ'_w (equal to θ'_w/t), with varying Ω and α are summarized in Table 1. Table 1 indicates that, similar to the flow visualization results, the wake width and structure remained relatively unchanged until $\alpha > 10$ deg. For $\alpha \geq 12$ deg, the wake became broadened dramatically and was accompanied by a very high level of fluctuation for the case of no rotation ($\Omega = 0$), suggesting that, with $\Omega = 0$, the LERC airfoil stalled at around 12 deg, in contrast to an $\alpha_{ss} = 14$ deg of a base airfoil.

The beneficial effects of high cylinder rotation on the airfoil flow can also be depicted through the surface pressure distributions (Fig. 3c). Figure 3c suggests that, for an LERC with $\Omega < 0.75$, the airfoil remained stalled (indicated by a uniform or flat surface pressure coefficient C_P distribution on the top of the airfoil surface). For $\Omega \geq 0.75$, the significant increase in C_P distribution indicated a reestablishment of an essentially reattached flow over most of the upper surface of the airfoil. Also, a large, well-developed suction peak existed at the leading edge of the airfoil and resulted in a delayed stall and an increased lift (Fig. 4). The flat plateau existing between $x/c \approx 0.1$–0.3 in C_P distribution for $\Omega = 0.75$ suggests the existence of a relatively large separation bubble on the airfoil's upper surface, followed by a turbulent separation toward the trailing edge of the airfoil. The variation of the coefficient of section lift C_l with cylinder rotation is summarized in Fig. 4. The stall angles of attack were found to be 16.5 and 18.5 deg for $\Omega = 1$ and 1.5, respectively, compared to $\alpha_{ss} = 14$ deg for a base airfoil. The stalling of the base airfoil set in rather abruptly, as shown by a sudden drop in the lift curve. For $\Omega \geq 1$, however, the stall was delayed and became more gentle, with an extended lift curve, but with no slope variation. An increase in C_l of about 30% for $\Omega = 1.5$ compared to that of a base airfoil was observed.

The influence of cylinder rotation on the growth and development of the boundary layer developed on the airfoil's upper surface was investigated at eight streamwise locations ($x/c = 0.075$–0.7) along the airfoil upper surface for $\alpha = 2$–18 deg and $\Omega = 0$–1. Typical results for $\alpha = 14$ and 16 deg at $x/c = 0.075$, 0.15, and 0.4 are presented in Fig. 5. For $\Omega < 0.3$, the level of turbulence fluctuation u' was higher than that of a base airfoil and decreased with increasing cylinder rotation. For $\Omega \geq 0.75$, the turbulence fluctuations in the boundary layer were greatly suppressed. Some of the velocity profiles developed on an LERC airfoil surface, especially in the leading-edge region of the airfoil, appeared fuller due to the additional momentum injection as compared to those of a base airfoil. The increase in the mean velocity u in the near-wall region is representative of the initial magnitude of the momentum injected, which dominates the extent to which the LERC boundary-layer control ends and the normal no-slip boundary-layer condition takes place. With $\Omega = 0$, the boundary layer separated at $x/c \leq 7.5\%$ and was thicker. The negative effects were attributed to the protrusion of the rotating cylinder ($d = 0.1c$) in the leading-edge region of the airfoil. The separated boundary layer, however, became reattached at higher cylinder rotation. For example, at $\alpha = 12$ deg with $\Omega \geq 0.3$, the boundary-layer separation was delayed up to $x/c \geq 70\%$ in comparison to $x/c < 60\%$ for a base airfoil. At $\alpha = 16$ deg with $\Omega = 0.75$, the poststalled boundary layer reattached onto the airfoil upper surface at around $x/c \geq 30\%$ and was accompanied by a much narrower boundary-layer thickness. Note that, due to the limitation of a hot-wire probe in the measurement of flow reversal, the boundary-layer velocity measurements downstream of the flow separation could only be used as a reference.

Figures 6a–6g summarize the variation of the boundary-layer momentum thickness θ_{bl} and its growth with Ω for $\alpha = 4$–16 deg. There was a decrease in θ_{bl} in general with increasing cylinder rotation. This was most pronounced for $\alpha \geq \alpha_{ss}$ (Figs. 6f and 6g). For example, at $\alpha = 16$ deg with $\Omega \geq 0.3$, there is a significant reduction in θ_{bl} in comparison to those of a base airfoil, implying a narrowly confined viscous effect and an increase in the momentum injection into the boundary layer, especially in the leading-edge region of the airfoil. With x up to $x/c \leq 50\%$, θ_{bl} grew linearly, but at a lower rate, except that for the case of $\Omega = 0$, compared to those of a base airfoil. The growth of θ_{bl}, $d\theta_{bl}/dx$, decreased with increasing cylinder rotation and was a nonlinear function of the angle of attack (Fig. 7).

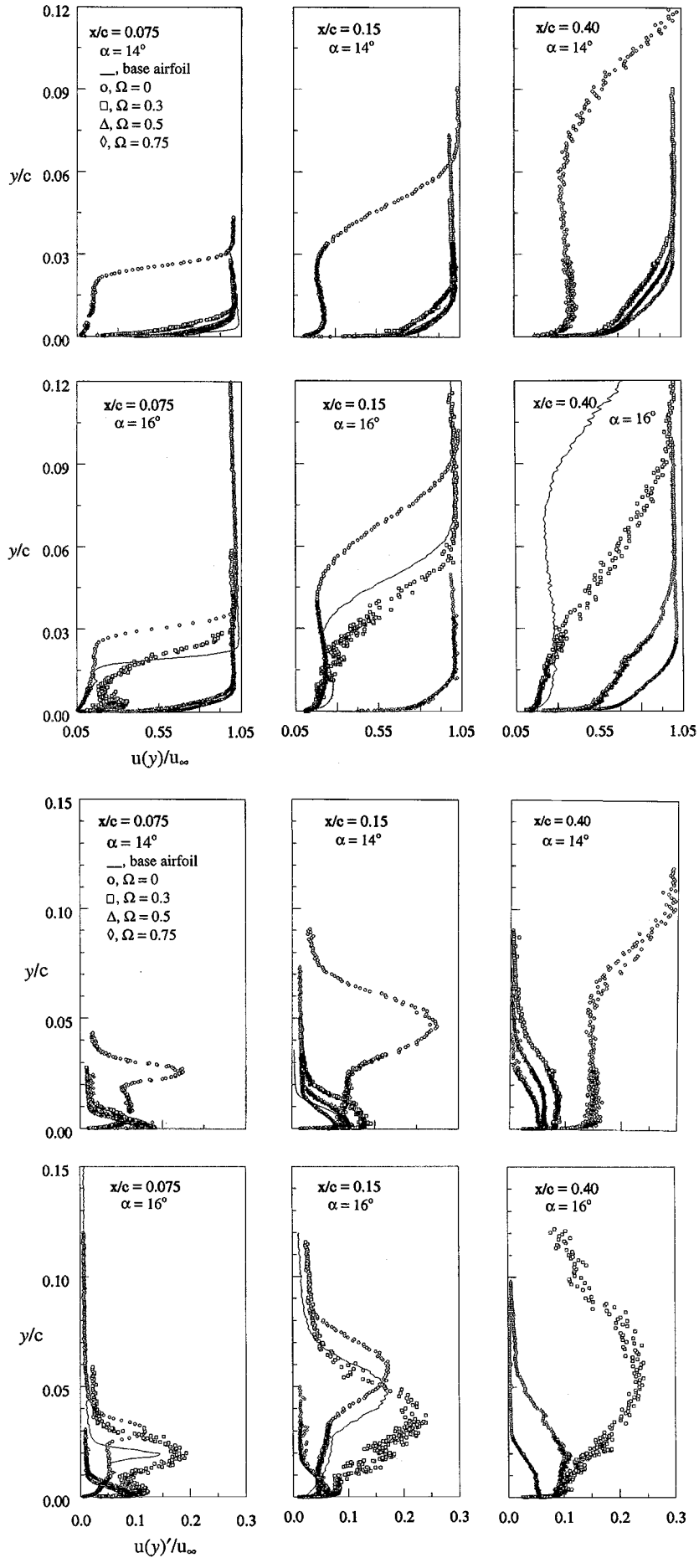

Fig. 5 Typical mean and fluctuating boundary-layer velocity profiles for $\alpha = 14$ and 16 deg.

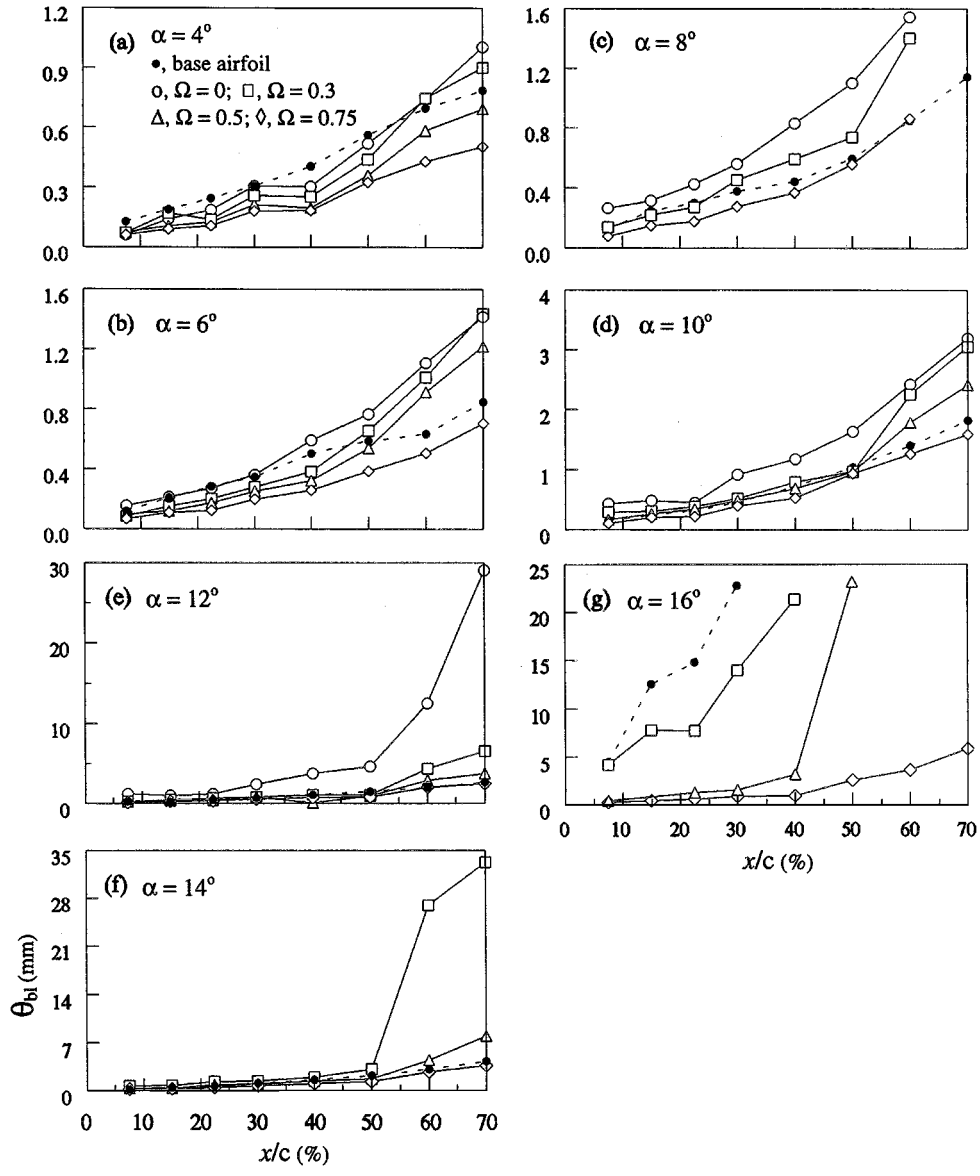

Fig. 6 Variation of θ_{bl} with Ω at different α.

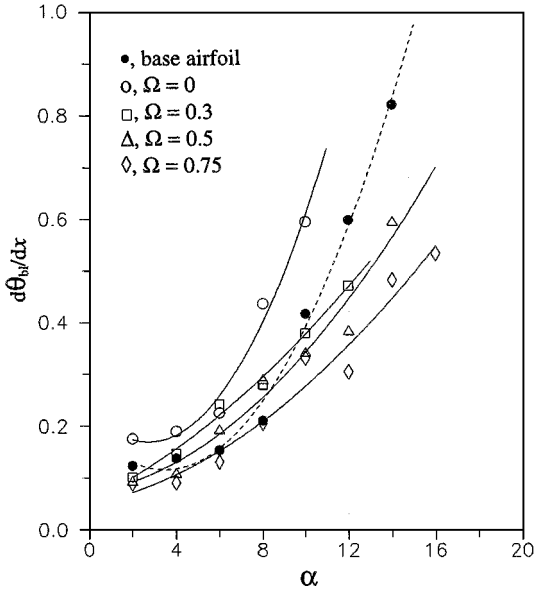

Fig. 7 Effect of Ω on $d\theta_{bl}/dx$.

Conclusions

The effects of leading-edge cylinder rotation on the boundary layer and wake, and the lift-to-drag ratio of a NACA 0015 airfoil, were quantified. With cylinder rotation, a delayed boundary-layer flow separation accompanied by a narrowed wake and an enhanced lift could be obtained. The effectiveness of LERC boundary-layer control is of particular importance for α considerably beyond the static-stall angle. The boundary-layer momentum thickness decreased with increasing cylinder rotation and grew linearly with the streamwise distance along the airfoil surface. The present measurements not only demonstrate the improved aerodynamic performance through a leading-edge circulation control device, but also provide typical data for computer model validations.

Acknowledgment

This work was supported by the Natural Sciences and Engineering Research Council of Canada. R. Saba is thanked for his help with the design of the rotating mechanism.

References

[1]Favre, A., "Contribution to the Study of Experiment of Hydrodynamic Movement in Two Dimensions," Ph.D. Dissertation, Dept. of Mechanics, Univ. of Paris, Paris, 1938.

[2]Chang, P. K., *Separation of Flow*, Pergamon, New York, 1970.

[3]Steele, B. N., and Harding, M. H., "Applications of Rotating Cylinders for Ship Maneuvering," *Journal of Naval Architecture*, Vol. 5, 1971, pp. 27–29.

[4]Tennant, J. S., Johnson, W. S., and Korthapalli, A., "Rotating Cylinder for Circulation Control on an Airfoil," *Journal of Hydronautics*, Vol. 10, 1976, pp. 102–105.

[5]Tennant, J. S., Johnson, W. S., and Keaton, D. D., "Boundary-Layer Flow from Fixed to Moving Surfaces Including Gap Effects," *Journal of Hydronautics*, Vol. 12, 1978, pp. 81–84.

[6]Mokhtarian, F., and Modi, V. J., "Fluid Dynamics of Airfoils with Moving Surface Boundary-Layer Control," *Journal of Aircraft*, Vol. 25, 1988, pp. 163–169.

[7]Kubo, Y., Modi, V. J., Yasuda, H., and Kato, K., "On the Suppression of Aerodynamic Instability Through the Moving Surface Boundary-Layer Control," *Journal of Wind Engineering and Industrial Aerodynamics*, Vol. 41, 1992, pp. 205–216.

[8]Kubo, Y., Modi, V. J., Kotsubo, C., Nayashida, K., and Kato, K., "Suppression of Wind-Induced Vibrations of Tall Structures Through Moving Surface Boundary-Layer Control," *Journal of Wind Engineering and Industrial Aerodynamics*, Vol. 61, 1995, pp. 181–194.

[9]Modi, V. J., Swinton, P. G., McMillan, K., Lake, P., Mullins, D., and Akutsu, T., "Moving Surface Boundary-Layer Control for Aircraft Operation at High Incidence," *Journal of Aircraft*, Vol. 18, No. 11, 1981, pp. 936–968.

[10]Modi, V. J., Mokhtarian, F., and Yokomizo, T., "Effect of Moving Surfaces on the Airfoil Boundary-Layer Control," *Journal of Aircraft*, Vol. 27, 1990, pp. 42–50.

[11]Modi, V. J., Mokhtarian, F., Fernando, M. S. U. K., and Yokomizo, T., "Moving Surface Boundary-Layer Control as Applied to Two-Dimensional Airfoils," *Journal of Aircraft*, Vol. 28, 1991, pp. 104–112.

[12]Modi, V. J., "Moving Surface Boundary-Layer Control: A Review," *Journal of Fluids and Structures*, Vol. 11, 1997, pp. 627–663.

[13]Ericsson, L. E., "Moving Wall Effect in Relation to Other Dynamic Flow Mechanics," *Journal of Aircraft*, Vol. 31, No. 6, 1994, pp. 1303–1309.

[14]Bhatia, J. C., Durst, F., and Jovanovic, J., "Corrections of Hot-Wire Anemometer Measurements Near Walls," *Journal of Fluid Mechanics*, Vol. 122, 1982, pp. 411–431.

[15]Lee, T., and Budwig, R., "Two Improved Methods for Low-Speed Hot-Wire Calibration," *Measurement Science and Technology*, Vol. 2, 1991, pp. 643–646.

Analytical Approximation for the Mechanics of Airplane Spin

W. F. Phillips* and E. A. Anderson†
Utah State University, Logan, Utah 84322-4130

Nomenclature

$b, \tilde{C}, c, S, \eta$	=	span, section normal force coefficient, chord, planform area, and efficiency factor of surface
I_{xx}, I_{yy}, I_{zz}	=	moments of inertia about the primary axes of roll, pitch, and yaw
ℓ, m, n	=	aerodynamic moments in roll, pitch, and yaw
R, V_d, Ω	=	spin radius, sink rate, and total spin rate
$\boldsymbol{r}, x, y, z$	=	position vector relative to the airplane c.g. and its conventional body-fixed components
T, ω_p	=	propeller thrust and angular velocity
$\boldsymbol{V}, u, v, w$	=	airplane's translational velocity vector and body-fixed components
$\boldsymbol{V}_r, V_N$	=	relative wind and its upward normal or negative z-component
W, X, Y, Z	=	airplane weight and the aerodynamic force components in the x, y, and z directions
ϕ, θ, σ	=	bank angle, elevation angle, and unconventional heading angle relative to the radial plane
$\boldsymbol{\Omega}, p, q, r$	=	airplane's rotational velocity vector and body-fixed components

Subscripts

b, e	=	body-fixed and Earth-oriented components
f, fh, fv	=	fuselage, fuselage horizontal planform, and fuselage vertical planform
h, p, r, v, w	=	horizontal stabilizer, propeller, rudder, vertical stabilizer, and wing

Received 16 May 2002; revision received 25 July 2002; accepted for publication 2 August 2002.

*Professor, Mechanical and Aerospace Engineering Department. Member AIAA.

†Assistant Professor, Mechanical and Aerospace Engineering Department. Senior Member AIAA.

Introduction

AIRPLANE spin was encountered very early in the history of aviation. In the early days of flight, airplane spin was the cause of many fatal accidents. Even today, spin is one of the primary causes of accidents in general aviation.[1,2] The aerodynamic forces and moments produced by the separated flow around a spinning airplane are highly nonlinear and quite complex. Thus, it is very difficult to predict accurately the unsteady motion of a spinning airplane from theoretical analysis alone.[3] Most of what is known about designing airplanes for spin resistance and spin recovery has been obtained from experimental investigation.[4–6] Nevertheless, some insight into the physics of airplane spin can be gained by examining the equations of motion for a fully developed steady spin.

Formulation

Consider the case of steady spin about a vertical axis as shown in Fig. 1. For convenience in writing the equations of motion, an unconventional set of Euler angles will be used. The bank angle and elevation angle are the same as those traditionally used by the aircraft community. As shown in Fig. 1, the heading angle used here, σ, is similar to the conventional azimuth angle, but is measured from the radial plane, not from north. This set of Euler angles describes the orientation of the airplane with respect to an Earth-oriented coordinate system that rotates with the airplane, has the x axis pointed toward the axis of the spin helix, and has the z axis pointed down. The airplane's translational and angular velocity vectors are easily described in this Earth-oriented coordinate system and, thus, can be transformed to conventional body-fixed coordinates using the well-known Euler angle transformation matrix[7]

$$\boldsymbol{V} = \begin{Bmatrix} 0 \\ -R\Omega \\ V_d \end{Bmatrix}_e \equiv \begin{Bmatrix} u \\ v \\ w \end{Bmatrix}_b = \begin{Bmatrix} -V_d \sin\theta - R\Omega \sin\sigma \cos\theta \\ V_d \cos\theta \sin\phi - R\Omega(\cos\sigma \cos\phi + \sin\sigma \sin\theta \sin\phi) \\ V_d \cos\theta \cos\phi + R\Omega(\cos\sigma \sin\phi - \sin\sigma \sin\theta \cos\phi) \end{Bmatrix}_b \tag{1}$$

$$\boldsymbol{\Omega} = \begin{Bmatrix} 0 \\ 0 \\ \Omega \end{Bmatrix}_e \equiv \begin{Bmatrix} p \\ q \\ r \end{Bmatrix}_b = \begin{Bmatrix} -\Omega \sin\theta \\ \Omega \cos\theta \sin\phi \\ \Omega \cos\theta \cos\phi \end{Bmatrix}_b \tag{2}$$

Applying these body-fixed velocity components to Euler's equations of motion[8] and choosing the body-fixed coordinate system to coincide with the primary inertial axes of the airplane gives